AIAA JOURNAL
Vol. 40, No. 1, January 2002

Magnetohydrodynamic Control of Hypersonic Flows and Scramjet Inlets Using Electron Beam Ionization

Sergey O. Macheret,* Mikhail N. Shneider,† and Richard B. Miles‡
Princeton University, Princeton, New Jersey 08544

The possibility of controlling scramjet inlets in off-design conditions by operating a near-surface magnetohydrodynamic (MHD) system upstream of the inlet is examined. The required electrical conductivity in air is supposed to be created by electron beams injected into the air from the vehicle along magnetic field lines. A simple model of a beam-generated ionization profile is developed and coupled with plasma kinetics, MHD equations, and two-dimensional inviscid flow equations. Calculations show that an MHD system with reasonable parameters could bring shocks back to the cowl lip when flying at Mach numbers higher than those for which the inlet was optimized. The MHD effect is not reduced to heating only because the work by $j \times B$ forces is a substantial part of the overall effect. Power requirements for ionizing electron beams could be lower than the electrical power extracted with MHD, so that a net power would be generated onboard. Problems associated with high Hall fields are discussed.

Nomenclature

a	=	parameter in Gaussian approximation of electron beam power deposition profile
B	=	magnetic field
$B_{\max}$	=	maximum value of the magnetic field
B_z	=	z component of the magnetic field
b	=	parameter in Gaussian approximation of electron beam power deposition profile
E_{eff}	=	effective electric field
E_v	=	nonequilibrium vibrational energy per unit volume
E_v^0	=	equilibrium vibrational energy per unit volume
E_x	=	x component of the electric field
$E_{x,\max}$	=	maximum value of x component of the electric field
E_y	=	y component of the electric field
e	=	electron charge
e_{tot}	=	total energy of the gas per unit volume
$\boldsymbol{H}$	=	column vector in Euler equations
$\dot{H}_{\text{inlet}}$	=	total enthalpy entering the inlet per unit time
h	=	flight altitude
$\hbar$	=	Planck's constant
I	=	ionization energy
$I_{m,k}$	=	excitation energy of the mth level of molecules of species k
$\boldsymbol{i}_x$	=	vector of unit length in x direction
$\boldsymbol{i}_z$	=	vector of unit length in z direction
j	=	electric current density
j_b	=	initial electron beam current density
j_y	=	y component of the current density
k	=	load factor
k_d	=	rate coefficient of collisional detachment of electrons from negative ions
L	=	electron beam energy loss function
L_{MHD}	=	length of magnetohydrodynamics (MHD) region
l_R	=	electron beam relaxation length
M	=	Mach number
$\dot{m}$	=	mass flow rate
N	=	number density of gas molecules
N_{O}	=	number density of oxygen atoms
n_e	=	electron number density
n_+	=	positive ion number density
n_-	=	negative ion number density
P	=	power dissipated in the external load per the unit volume of the gas
P_b	=	power deposited by the electron beam in the gas
P_J	=	joule dissipation rate
$P_{j\times B}$	=	push power
P_{MHD}	=	MHD generated power
P_{VT}	=	heating rate due to vibration–translation (VT) relaxation
P_v	=	energy addition rate into vibrational mode
p	=	pressure
p_{tot}	=	total pressure at the inlet
p_0	=	pressure in the freestream
Q_b	=	power deposited per unit volume by the electron beam
Q_{VT}	=	heating rate per unit volume due to VT relaxation
Q_v	=	power deposited per unit volume into vibrational excitation
q_i	=	ionization rate due to electron beam
S	=	MHD interaction parameter
T	=	translational–rotational gas temperature
T_v	=	vibrational temperature
$\boldsymbol{U}$	=	column vector in Euler equations
u	=	x component of gas velocity
$\tilde{u}$	=	effective electron–ion velocity across the magnetic field taking into account ion slip
V_{MHD}	=	effective volume of MHD interaction region
v	=	z component of gas velocity
W_i	=	energy cost of ionization, that is, the loss of electron beam energy per each newly generated electron in the plasma
w	=	parameter in Gaussian approximation of electron beam power deposition profile
$\boldsymbol{X}$	=	column vector in Euler equations
x	=	coordinate
$\bar{x}$	=	transformed x coordinate
y	=	coordinate
Z	=	column vector in Euler equations
z	=	coordinate
z_b	=	coordinate along the wall
z_m	=	parameter in Gaussian approximation of electron beam power deposition profile

Presented as Paper 2001-0492 at the AIAA 39th Aerospace Sciences Meeting, Reno, NV, 8–11 January 2001; received 11 March 2001; revision received 14 August 2001; accepted for publication 14 August 2001.

*Research Scientist, Department of Mechanical and Aerospace Engineering, D-414 Engineering Quadrangle; Macheret@princeton.edu. Associate Fellow AIAA.

†Research Staff Member, Department of Mechanical and Aerospace Engineering, D-414 Engineering Quadrangle. Member AIAA.

‡Professor, Department of Mechanical and Aerospace Engineering, D-414 Engineering Quadrangle. Fellow AIAA.

$z_{\max}$ = maximum value of z coordinate in the computational domain
$\bar{z}$ = transformed z coordinate
α = Townsend ionization coefficient
β = electron–ion recombination rate coefficient
β_{ii} = ion–ion recombination rate coefficient
$\boldsymbol{\Gamma}_e$ = flux of electrons
$\boldsymbol{\Gamma}_+$ = flux of positive ions
$\boldsymbol{\Gamma}_-$ = flux of negative ions
ε = energy of beam electrons
ε_b = initial energy of beam electrons
ε_{int} = internal energy per unit mass
ε_v = nonequilibrium vibrational energy per molecule
ε_v^0 = equilibrium vibrational energy per molecule
η_v = fraction of the joule dissipation rate spent on vibrational excitation of molecules
μ_e = electron mobility
ν_a = electron attachment frequency, that is, the number of attachments per unit time
ρ = gas density
σ = effective electrical conductivity
$\sigma_{m,k}$ = cross section for electron impact excitation of the mth level of molecules of species k
τ_{VT} = nitrogen vibrational relaxation time
χ = ratio between the MHD-generated electrical power and the total enthalpy entering the inlet per unit time
Ω_e = electron Hall parameter
Ω_+ = ion Hall parameter
ω_0 = vibrational frequency corresponding to transition between the ground and the first excited vibrational state of nitrogen molecule

I. Introduction

A NUMBER of applications of magnetohydrodynamic (MHD) technology to hypersonics have been suggested recently.[1–21] These applications include MHD power generation,[1–11] MHD energy bypass (AJAX),[1–7,12,13] and scramjet inlet control.[1–4,14–18] It is the latter application that this paper is focused on. The principal idea, discussed most recently in Refs. 14–18, is that, by creating a near-surface magnetic field and placing a proper set of electrodes at some location inside the scramjet inlet or upstream of it, flow pattern could be changed due to the action of both $\boldsymbol{j} \times \boldsymbol{B}$ forces and joule heating. One specific task would be to assist the scramjet in offdesign conditions. If an aircraft and the engine inlet geometry have been optimized for a certain Mach number, then flying at a different Mach number could create problems. Those problems may include shocks entering the engine, flow separation, oscillations, and unstart. As discussed in Refs.1, 4, 5, and 7 and especially demonstrated in some detail in Refs. 16–18, the MHD region upstream of the inlet could potentially affect the flow in offdesign cases and bring bow shock back to its optimum location at the cowl lip. However, the analysis of Refs. 16–18 implicitly assumed that the air is highly conductive. For the magnetic interaction parameter to reach 0.5–1, as was assumed in Refs. 16–18, and at modest magnetic fields, the ionization degree has to be of the order of 10^{-4}. Ionization level that high could be achieved at temperatures of several thousand Kelvin with alkali seed. Meanwhile, at flight Mach numbers below about Mach 12, static temperature downstream of the oblique bow shock is much lower, from several hundred to perhaps a thousand Kelvin. Thus, the ionization required for MHD control has to be created artificially. Because the ionization would not be free, the power budget for sustaining the ionization becomes a critical factor.

In earlier papers,[8–11,19–22] we analyzed various nonequilibrium ionization methods and concluded that high-energy electron beams are the most efficient ionizers. We have suggested a concept of hypersonic MHD channels with ionization by electron beams.[8–11,19–21] Theoretical and computational modeling of these channels showed that substantial amounts of enthalpy could be added to or extracted from the flow in an energy-efficient manner, although a number of issues have to be resolved to fully assess the viability of the concept. In the present paper, we apply the concept of cold-air supersonic MHD generators with electron-beam ionization to control of external flows. The specific problem of interest is scramjet inlet operation at offdesign Mach numbers.

As a first step, we restrict ourselves to inviscid calculations, scaled-down geometry, and a single off-design set of conditions.

II. Model Description

A. Gasdynamic and MHD Equations

We consider hypersonic gas flow along the two ramps with 10- and 20-deg angles before the inlet with forward-shifted cowl lip, as shown in Figs. 1 and 2. The flow is two dimensional in the x, z plane. Cases both without and with MHD influence on the flow are computed. In MHD cases, both magnetic field and ionizing electron beam are directed parallel to z axis.

The set of Euler equations in Cartesian coordinates, together with the ideal gas equation of state, the simple model of ideal Faraday MHD generator, and the vibrational relaxation equation, is

$$\frac{\partial}{\partial t}\boldsymbol{U} + \frac{\partial}{\partial x}\boldsymbol{X} + \frac{\partial}{\partial z}\boldsymbol{Z} = \boldsymbol{H} \tag{1}$$

$$\boldsymbol{U} = \begin{Vmatrix} \rho \\ \rho u \\ \rho v \\ e_{\text{tot}} \\ E_v \end{Vmatrix}, \qquad \boldsymbol{X} = \begin{Vmatrix} \rho u \\ \rho u^2 + p \\ \rho v u \\ (e_{\text{tot}} + p)u \\ E_v u \end{Vmatrix}$$

$$\boldsymbol{Z} = \begin{Vmatrix} \rho v \\ \rho u v \\ \rho v^2 + p \\ (e_{\text{tot}} + p)v \\ E_v v \end{Vmatrix}, \qquad \boldsymbol{H} = \begin{Vmatrix} 0 \\ j_y B_z \\ 0 \\ Q \\ Q_v - Q_{\text{VT}} \end{Vmatrix} \tag{2}$$

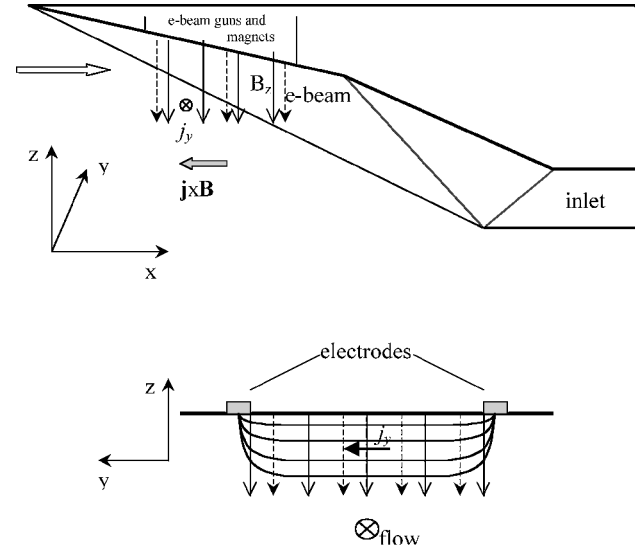

Fig. 1 Scramjet inlet with shocks ideally converging on the cowl lip (the flow is from left to right) and schematic MHD configuration in x, z and y, z planes.

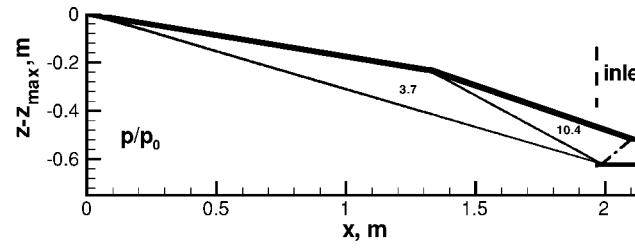

Fig. 2 Computed shock configuration at Mach 6, with shocks converging on the cowl lip.

$$p = (\gamma - 1)\rho\varepsilon_{\text{int}} \tag{3}$$

$$e_{\text{tot}} = \rho\left[\varepsilon_{\text{int}} + (u^2 + v^2)/2\right] \tag{4}$$

The source term in the total energy equation is

$$Q = -P - Q_v + Q_{\text{VT}} + Q_b \tag{5}$$

where

$$P = k(1-k)\sigma u^2 B_z^2 \tag{6}$$

is the power from the unit volume of the gas dissipated in the external load. The vibrational excitation term Q_v can be expressed as a fraction η_v of the joule heating rate:

$$Q_v = \eta_v j_y^2 \big/ (e\mu_e n_e) \tag{7}$$

The fraction η_v is a function of the local reduced electric field, $E_{\text{eff}}/N = (E_y - uB_z)/N$. The fraction η_v was taken from Ref. 23, where it has been tabulated as a function of E/N on the basis of the solution of Boltzmann kinetic equation for plasma electrons.

The remaining energy addition and dissipation terms are

$$Q_{\text{VT}} = \frac{E_v - E_v^0(T)}{\tau_{\text{VT}}(T)} \tag{8}$$

heating rate per unit volume due to vibration–translation (VT) relaxation and q_h, power deposited per unit volume by the electron beam.

Nonequilibrium and equilibrium vibrational energy can be expressed through the respective temperatures by the Planck formula:

$$E_v = N\varepsilon_v = N\frac{\hbar\omega_0}{\exp(\hbar\omega_0/T_v) - 1}$$

$$E_v^0 = N\varepsilon_v^0 = N\frac{\hbar\omega_0}{\exp(\hbar\omega_0/T) - 1} \tag{9}$$

where $\hbar w_0$ is the lowest vibrational quantum of nitrogen molecules and the temperatures are expressed in energy units.

Nitrogen vibrational relaxation time is sensitive to both temperature and the concentration of atomic oxygen, and it was taken as in Refs. 8–11:

$$\frac{1}{\tau_{\text{VT}}} = N \cdot \left[7 \times 10^{-10} \exp\left(-\frac{141}{T^{\frac{1}{3}}}\right) + \frac{N_{\text{O}}}{N} \cdot 5 \times 10^{-22} \exp\left(-\frac{128}{T^{\frac{1}{2}}}\right)\right] \tag{10}$$

where N_{O} and N are expressed in cubic centimeter per second.

The electric field and current density can be expressed in terms of the load factor k (Refs. 8–11 and 24):

$$E_y = (1-k)uB_z, \qquad j_y = \sigma uB_z(1-k) \tag{11}$$

The effective electrical conductivity, taking into account ion slip, is[24]

$$\sigma = \frac{e\mu_e n_e}{1 + \Omega_e\Omega_+} \tag{12}$$

Computations were performed by a second-order MacCormack method (see Ref. 25) on a rectangular grid. For this, physical coordinates x, z were transformed into $\bar{x}$, $\bar{z}$:

$$\bar{x} = x, \qquad \bar{z} = z/z_b(x), \qquad \bar{z} \in [0, 1] \tag{13}$$

where $z_b(x)$ is the coordinate along the wall. The results presented here correspond to a grid size of 250×150. Variation of the results with grid size is discussed at the end of Sec. III.

B. Plasma Model

The plasma is modeled as consisting of electrons and positive and negative ions, whose number densities n_e, n_+, n_- obey the quasi neutrality: $n_+ \approx n_e + n_-$. The set of equations for kinetics of charge species, accounting for electron beam-induced ionization rate (q_i term), ionization rate due to plasma electrons with Townsend ionization coefficient α depending on the local reduced electric field, $E_{\text{eff}}/N = (E_y - uB_z)/N$, attachment of electrons to molecules with formation of negative ions (frequency ν_a), collisional detachment of electrons from negative ions (rate constant k_d), and electron–ion and ion–ion recombination (rate coefficients β and β_{ii}, respectively), is

$$\frac{\partial n_e}{\partial t} + \operatorname{div}\boldsymbol{\Gamma}_e = \alpha|\boldsymbol{\Gamma}_e| + q_i + k_d N n_- - \nu_a n_e - \beta n_+ n_e$$

$$\frac{\partial n_+}{\partial t} + \operatorname{div}\boldsymbol{\Gamma}_+ = \alpha|\boldsymbol{\Gamma}_e| + q_i - \beta_{ii} n_- n_+ - \beta n_+ n_e$$

$$\frac{\partial n_-}{\partial t} + \operatorname{div}\boldsymbol{\Gamma}_- = -k_d N n_- + \nu_a n_e - \beta_{ii} n_- n_+ \tag{14}$$

In the case of ideal Faraday generator, there are no drift fluxes along either the x or z axes, and therefore, the fluxes of charged species in x, z plane can be written simply as $\boldsymbol{\Gamma}_{e,+,-}(x, z) = n_{e,+,-}(\tilde{u}\cdot\boldsymbol{i}_x + v\cdot\boldsymbol{i}_z)$, where $\tilde{u}$ is the effective electron–ion velocity across magnetic field taking into account ion slip,[10,11]

$$\tilde{u} = u/[1 + (1-k)\Omega_e\Omega_+] \tag{15}$$

The initial conditions for plasma components are $n_{e,+,-}(x, z, t = 0) = 0$. The boundary conditions are $n_{e,+,-}(x = 0, z, t) = n_{e,+,-}(x, z = z_b(x), t) = 0$.

Rate coefficients of electron–ion and ion–ion recombination and of electron attachment and detachment processes, discussed in Refs. 8–10, were taken from Refs. 26 and 27. Because some of those rate coefficients depend on electron temperature T_e, it is important to calculate the electron temperature in the modeling. In our computations, electron temperature was determined from the tabulated data on electron diffusion and mobility coefficients of Ref. 23. In that paper, the diffusion and mobility coefficients are listed as functions of E/N, determined from experimental data and extrapolation based on solution of the Boltzmann kinetic equation for electrons in air.

C. Power Deposition and Ionization by the Electron Beam

To model hypersonic MHD systems properly, equations describing electron beam propagation and beam-generated ionization have to be coupled with gasdynamic and electromagnetic equations. In our earlier work,[8–10,21] we used the so-called forward–backward approximation[28] for electron beam propagation into gases and beam-generated ionization. This method is quite accurate, and it can be (and, in fact, was[8,21]) coupled with Navier–Stokes and MHD equations. However, computational demands of the full forward–backward method, when coupled with gasdynamic and MHD equations, are prohibitive. Therefore, a simple but accurate way to predict ionization profiles should be found.

Having analyzed the physics of the ionization processes, we concluded that in a uniform gas the ionization rate profile has to be close to Gaussian. Indeed, ionization of molecules by electron impact is inefficient both at low and high (above 1 keV) electron energies.[29,30] The maximum of the ionization cross section corresponds to electron energy of several hundred electron volts.[29,30] In this energy range, and even above it, the probability of backscattering is substantial, and there are both forward and backward electron fluxes exchanging electrons between them. The resulting motion is very much like diffusion.

Another way of looking at this is to note that average energy transferred in collisions of energetic electrons with molecules, comparable with the ionization energy, is about 1–30 eV, which is much smaller than the beam electron energy. Hence, the energy relaxation of the energetic beam should be close to a small-step random walk in energy space. Because electron stopping distance is nearly proportional to the initial energy, the diffusion in energy space translates into spatial diffusion. Diffusion profiles are well known to be Gaussian, and, in the case of electron beam propagation, this can be tested against forward–backward calculations.

Indeed, we found that forward–backward energy deposition Q_b and ionization profiles are very close to Gaussian:

$$Q_b = a + (b/w)\exp\left\{-2[z_b(x) - z - z_m]^2 \big/ w^2\right\} \tag{16}$$

where $z_m \approx l_R/3.21$, $w \approx 1.64 z_m$, and $l_R(\varepsilon_b, N)$ is the beam relaxation length. There are two additional conditions for determining the constants a and b:

$$Q_b(l_R) = 0, \qquad \int_0^{l_R} Q_b(z)\,\mathrm{d}z = \frac{|j_b|\varepsilon_b}{e} \tag{17}$$

The relaxation length can be found using the loss function

$$L(\varepsilon, N) = \sum_{m,k} I_{m,k} N_k \sigma_{m,k}(\varepsilon) \tag{18}$$

We denote the cross section for excitation of the mth level of molecules of species k by $\sigma_{m,k}(\varepsilon)$ and the corresponding excitation energy by $I_{m,k}$. Ionization of the molecules is also included in L. N_k is the density of molecules of species k. We consider air as a mixture of two species: N_2:$O_2 = 4$:1. The profiles of both beam-induced energy deposition and ionization rate

$$q_i(x, z) \approx Q_b(x, z)/(eW_i) \tag{19}$$

where $W_i = 34$ eV is the energy cost of ionization by high-energy beam, can be easily found from Eqs. (16–18) if the density N is constant. It turns out that the quasi-Gaussian profile (16) works well even for nonuniform density profiles. In that case, the beam relaxation length is a local parameter found from the equation

$$\frac{\mathrm{d}\varepsilon}{\mathrm{d}z} = -L(\varepsilon, N), \qquad N = N(z) \tag{20}$$

The boundary condition at the beam injection point with the coordinate $z = z_b(x)$ is

$$\varepsilon = \varepsilon_b \qquad \text{at} \qquad z = z_b(x) \tag{21}$$

Equation (20) is solved, and the point z where $\varepsilon(z) \approx I$, the ionization energy, is determined. This defines the relaxation length

$$l_R(x) = z_b(x) - z \tag{22}$$

so that $\varepsilon(z) \approx I$.

The electron beam-generated power deposition and ionization profiles computed with this simple method were found to be within 10–20% of those computed with the forward–backward method.

III. Computed Cases

The inlet geometry was first optimized for Mach 6: The location of the cowl lip was chosen so that both oblique shocks would together reach the lip, and the reflected shock would fall right on the corner between the second ramp and the engine. This configuration is shown in Fig. 2. The freestream conditions correspond to the altitude of 27 km.

Next, the flow velocity was increased to Mach 8 for the same geometry. To keep the dynamic pressure at the inlet about the same as at Mach 6, the flight altitude would have to be increased, and all Mach 8 cases were run for an altitude of 30 km. As seen in Fig. 3, the shock would now make contact with the cowl farther downstream, and, although the flow past that point was not computed, multiple reflected shocks, boundary-layer growth, and flow separation could be expected, which is quite undesirable.

To learn whether an MHD system could bring the flow closer to the design point, an ideal Faraday generator system with the loading parameter $k = 0.5$ was put near the surface of the first ramp. Both magnetic field and electron beam were assumed to be directed

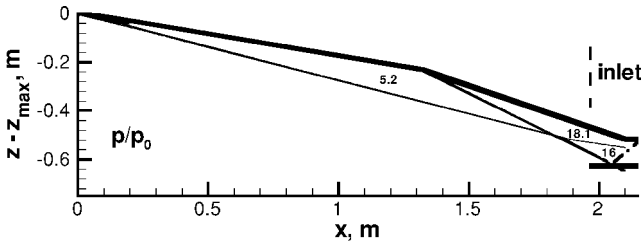

Fig. 3 Computed flow in Mach 8, $h = 30$ km, case without MHD; shocks move inside the engine.

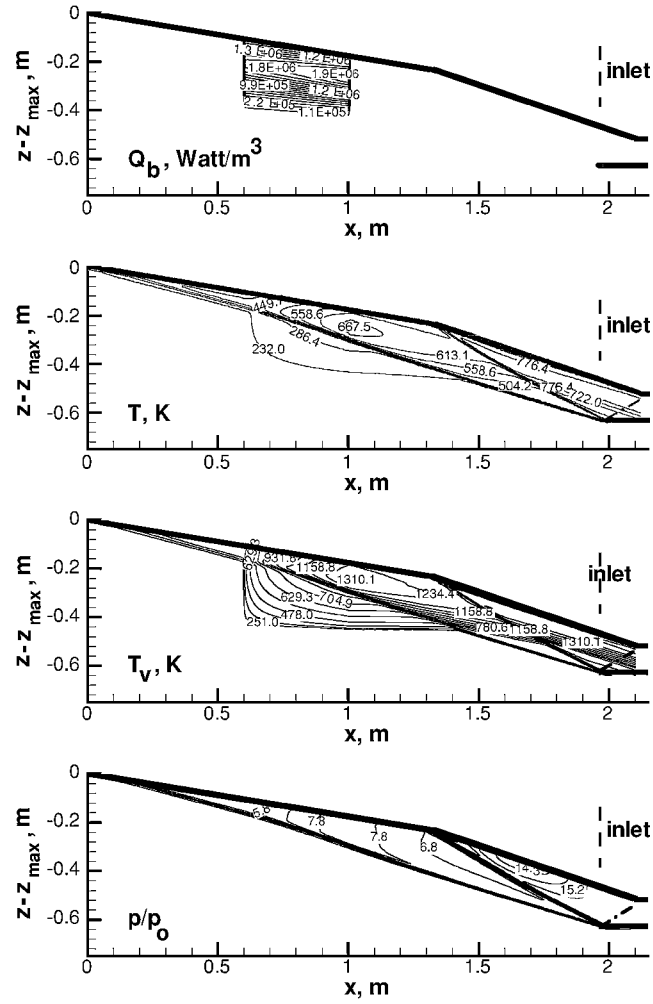

Fig. 4 Computed electron-beam energy deposition rate, gas temperature, vibrational temperature, and static pressure in Mach 8 case with MHD. MHD and beam parameters: $k = 0.5$, $j_b = 1.05$ mA/cm^2, $\varepsilon_b = 10$ keV, and $B = 3$ T.

downward along z axis. Both B field and electron beam were assumed uniform along x within the region $0.6 \le x \le 1$ m and to be equal to zero elsewhere. The presumed MHD configuration in x, z and y, z planes is shown schematically in Fig. 1. The B field profile along z axis was Gaussian:

$$B = B_{\max} \exp\left\{-\frac{[z_b(x) - z]^2}{(35\ \mathrm{cm})^2}\right\}$$

with the maximum of $B_{\max} = 3$ tesla at the wall. Electron beam energy and current density were adjusted to move the shocks at Mach 8 back to the cowl lip.

As seen in Fig. 4, with the beam parameters $j_b = 1.05$ mA/cm^2 and $\varepsilon_b = 10$ keV, and with the length of the MHD region of $L_{\mathrm{MHD}} = 0.4$ m, both shocks could be moved back to the cowl lip. However, their angles of incidence are slightly different from those in the Mach 6 case, so that the reflected shock would not exactly follow the design line. Perhaps an additional adjustment with an internal MHD or other control system would be required.

Details of charged species and vibrational temperature profiles in the computed MHD case are shown in Figs. 4–6. As seen in Fig. 5, inside the MHD region with electron beam ionization, electron density is of the order of $(1 - 3) \times 10^{12}$ cm^{-3}, controlled by beam-induced ionization and electron–ion recombination. The corresponding maximum ionization fraction is 5×10^{-6}, and the maximum conductivity is 1.9 mho/m. Attachment is insignificant, and the negative ion density is small. Downstream of the beam-ionized MHD region, electrons disappear almost immediately, but the wake of about 2.3×10^{10} cm^{-3} negative ions persists and enters the engine (Fig. 6).

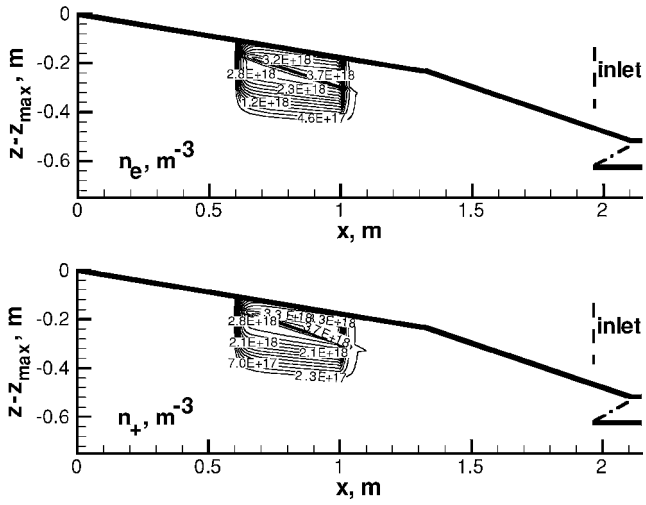

Fig. 5 Computed number densities of electrons and positive ions in the MHD region for the case shown in Fig. 4.

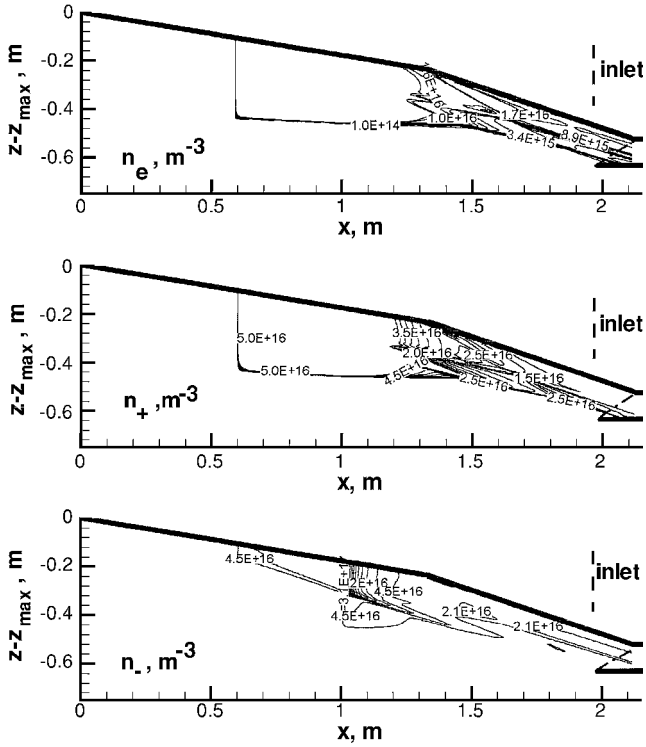

Fig. 6 Computed number densities charged species outside of the MHD region for the case shown in Fig. 4.

The value of MHD interaction parameter averaged over the volume V_{MHD} of MHD region

$$S = \frac{L_{\mathrm{MHD}}}{V_{\mathrm{MHD}}} \int_{V_{\mathrm{MHD}}} \frac{\sigma B_z^2}{\rho u}\,\mathrm{d}V$$

is about 0.11 in this case.

Vibrational temperature (Fig. 4) does exceed the gas temperature, but the degree of nonequilibrium and the enthalpy content of the vibrational mode are not high. Vibrational relaxation in this flow is very slow because of low temperature and density and because concentration of oxygen atoms would be low due to short residence time. Oxygen atoms are produced by direct dissociation of oxygen molecules by high-energy beam electrons. Additionally, beam electrons dissociate nitrogen, and, if the gas temperature reaches 600–700 K, oxygen atoms are produced in the reaction $\mathrm{N} + \mathrm{O}_2 \rightarrow \mathrm{NO} + \mathrm{O}$. Because the energy threshold for dissociation is comparable with that for ionization, the beam-induced dissociation and oxygen atom production rate can be estimated as approximately equal to the ionization rate, which in this case is about 4×10^{17} cm$^{-3} \cdot$ s^{-1}. An additional channel of production of O atoms is dissociative attachment of low-energy plasma electrons: $e + \mathrm{O}_2 \rightarrow \mathrm{O} + \mathrm{O}^-$. However, in all computed cases, attachment rate was at least an order of magnitude lower than the ionization rate (so that the ionization is balanced by electron–ion recombination). Therefore, the beam-induced ionization rate can serve as a good approximation for the O atom production rate.

O atoms could be destroyed in three-body processes such as $\mathrm{O} + \mathrm{O}_2 + \mathrm{M} \rightarrow \mathrm{O}_3 + \mathrm{M}$, $\mathrm{O} + \mathrm{O} + \mathrm{M} \rightarrow \mathrm{O}_2 + \mathrm{M}$, and $\mathrm{O} + \mathrm{N} + \mathrm{M} \rightarrow \mathrm{NO} + \mathrm{M}$. However, with the gas number density of 10^{18} cm^{-3} or so, these recombination processes would take at least 10 ms, whereas the flow residence time in the 0.4–1.1-m-long MHD channel is only 0.2–0.6 ms. The reaction $\mathrm{O} + \mathrm{N}_2 \rightarrow \mathrm{NO} + \mathrm{N}$ has high activation energy and is too slow at low vibrational and gas temperatures occurring in our cases. However, the reaction $\mathrm{N} + \mathrm{O}_2 \rightarrow \mathrm{NO} + \mathrm{O}$ is significant at gas temperatures of 500–700 K. Thus, a reasonable estimate of O atom density can be done by putting their production rate equal to the beam-induced ionization rate and neglecting all chemical removal processes, so that the produced atoms simply move with the flow. Therefore, the relative concentration of oxygen atoms should reach about $N_{\mathrm{O}}/N \approx (1-3) \times 10^{-4}$.

With gas temperatures in the range 400–800 K and O atom density quite low, nitrogen vibrational relaxation time will be longer than 10 ms. Therefore, vibrational temperature will keep growing along the MHD region and could be quite high at the exit.

Note that effects of chemistry and vibrational relaxation may be more pronounced when linear dimensions are scaled up, due to increased residence times. This issue will have to be addressed in future.

Table 1 lists some important parameters in computed cases:

$$P_b = \int_0^{x_{\max}} \int_0^{z_{\max}} Q_b\,\mathrm{d}x\,\mathrm{d}z$$

is the power deposited by electron beam,

$$P_{\mathrm{MHD}} = \int_0^{x_{\max}} \int_0^{z_{\max}} k u j_y B_z\,\mathrm{d}x\,\mathrm{d}z$$

is the MHD-generated electric power,

$$P_{j \times B} = \int_0^{x_{\max}} \int_0^{z_{\max}} u B_z j_y\,\mathrm{d}x\,\mathrm{d}z$$

is the push power,

$$P_J = \int_0^{x_{\max}} \int_0^{z_{\max}} (1-\eta_v)(1-k) u B_z j_y\,\mathrm{d}x\,\mathrm{d}z$$

is the joule dissipation rate,

$$P_v = \int_0^{x_{\max}} \int_0^{z_{\max}} \eta_v (1-k) u B_z j_y\,\mathrm{d}x\,\mathrm{d}z$$

is the energy addition rate into vibrational mode, and

$$P_{\mathrm{VT}} = \int_0^{x_{\max}} \int_0^{z_{\max}} Q_{\mathrm{VT}}\,\mathrm{d}x\,\mathrm{d}z$$

is the heating rate due to VT relaxation. All quantities are per unit length in the y direction.

The power cost of ionization is seen in the Table 1 to be quite low compared with other power budget components, including the generated electric power. Thus, the ionizing electron beams could be powered by a fraction of generated power, and a substantial portion of that power could be used for other purposes.

Another observation from Table 1 is that the rate of work done by the $\boldsymbol{j} \times \boldsymbol{B}$ force is quite a substantial part of the power budget. In other words, nonthermal, nonentropy-generating MHD effects are important in this case.

As seen in Table 1, MHD operation is accompanied by total pressure losses, due to entropy-generating joule dissipation: The total

Table 1 Various quantities in computed cases

Case[a]	p_{tot}, 10^5 Pa	P_b, MW/m	P_{MHD}, MW/m	$P_{j\times B}$, MW/m	P_J, MW/m	P_v, MW/m	P_{VT}, MW/m	$E_{y,\max}$, kV/m	$E_{x,\max}$, kV/m
$M=6$, $h=27$ km	2.06								
$M=8$, no MHD	2.926								
$M=8$, MHD $k=0.5$	2.017	0.121	3.65	7.3	2.21	1.44	0.0784	3.47	38.1
$M=8$, MHD $k=0.9$	2.023	1.66	3.91	4.34	0.34	0.095	0.002	0.72	7.98

[a]All Mach 8 cases correspond to an altitude of 30 km.

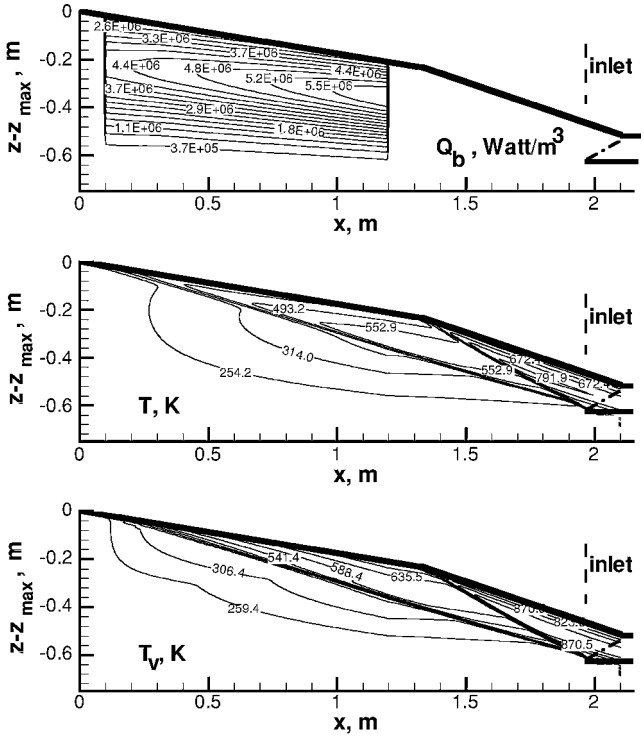

Fig. 7 Computed electron beam energy deposition rate, gas temperature, vibrational temperature, and static pressure in Mach 8 case with MHD. MHD and beam parameters: $k=0.9$, $j_b=4.2$ mA/cm^2, $\varepsilon_b=125$ keV, and $B=3$ T.

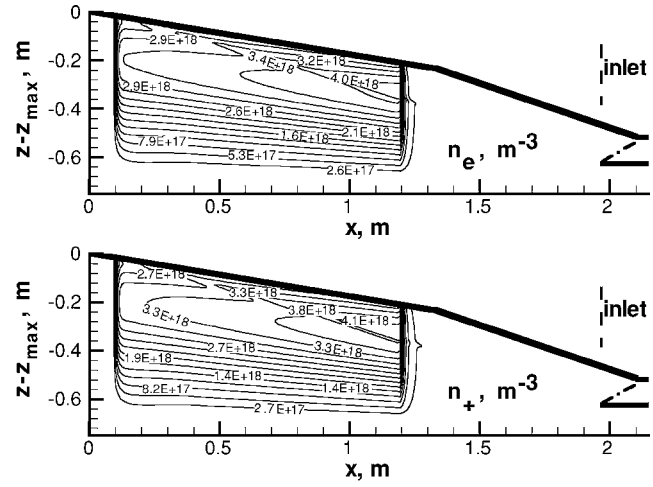

Fig. 8 Computed number densities of electrons and positive ions in the MHD region for the case shown in Fig. 7.

pressure at the cowl lip at Mach 8 drops from 2.9×10^5 Pa without MHD to 2.0×10^5 Pa with MHD. Note, however, that both the total pressure at the cowl lip and the mass flow rate at Mach 8 with MHD are essentially the same as at Mach 6 without MHD, so that the engine can operate as it did at Mach 6, but with the vehicle flying much faster. Additionally, when assessing advantages and flaws of MHD control, one has to bear in mind that without MHD, multiple shocks would exist in the inlet, resulting in a large decrease in total pressure from its value of 2.9×10^5 Pa at the cowl lip and also leading to boundary-layer separation and engine unstart. In this paper, we have not computed the flow downstream of the cowl lip due to its complexity in the non-MHD case. Evaluation of the MHD control approach should be done after a complete analysis of both MHD and non-MHD cases, which is outside the scope of this work.

Another way of stating that the MHD device causes total pressure losses due to entropy generation is to say that this device increases drag. To calculate this additional drag, full-configuration flow should be computed in both MHD and non-MHD cases. As already stated, full-configuration analysis was not done in this paper, primarily due to the complexity of the non-MHD case with multiple shocks, flow separation, and engine unstart. Thus, the comparison of advantages and drag penalty associated with MHD control is left to future work.

One reason for concern is a large value of Hall electric field, reaching $E_{x,\max}=38.1$ kV/m. In conventional high-temperature alkali-seeded MHD channels, the maximum Hall field is about 5–20 kV/m. At higher fields, arcing between the neighboring electrode segments starts. The reason for the high Hall field in our case is that the conductivity is not free and has to be created by electron beams. Because the electron beam power should be substantially less than the generated electric power, the conductivity has to be quite low. This, and the relatively short MHD region, dictates the need to have a strong magnetic field and the loading parameter considerably less than 1. As a result, the Hall parameter is high, of the order of 10, and the Hall field, $E_x=\Omega\cdot(1-k)uB$ is strong. Note that cold-air MHD channels with externally controlled ionization, where the ionization rate is uncoupled from heating, are quite different from conventional high-temperature seeded channels. The threshold Hall field for the onset of arcing between anode segments in nonequilibrium cold-air channels have never been explored, and it may well be that the threshold field is higher than the 5–20 kV/m. Nevertheless, the calculated field $E_{x,\max}=38.1$ kV/m is a reason for concern.

Reduction in this field could be achieved by increasing the loading parameter. To keep the overall MHD effect at the same level as before, the conductivity would have to be increased by using more powerful electron beams, and the MHD region would have to be longer. To check this idea, calculations were run with the loading parameter $k=0.9$. As shown in Figs. 7–9, by stretching the MHD region to $L_{\text{MHD}}=1.1$ m and increasing both current density and energy of the electron beam to $j_b=4.2$ mA/cm^2 and $\varepsilon_b=12.5$ keV, both shocks could be again moved back to the cowl lip. The ionization fraction is somewhat higher than in the $k=0.5$ case, reaching 6.3×10^{-6}, and the corresponding maximum conductivity is 2.4 mho/m. The value of MHD interaction parameter S, defined earlier, is 0.17 in this case. As seen in Table 1, electron beams would now consume a large fraction of the generated electrical power, although the balance is still positive. One has to keep in mind, though, that increasing the beam current density could create problems with beam injection windows. If these technical issues could be resolved, the Hall field would be substantially reduced: In this case, $E_{x,\max}\approx8$ kV/m, which might be acceptable.

Table 2 lists mass flow rate $\dot{m}$; total enthalpy entering the inlet per unit time $\dot{H}_{\text{inlet}}$; the difference between the total enthalpy carried by the mass flow $\dot{m}$ in the freestream and $\dot{H}_{\text{inlet}}$, $\Delta\dot{H}$; the difference

Table 2 Quantities calculated per unit length in *y* direction

Case[a]	$\dot{m}$, kg/m × s	$\dot{H}_{\text{inlet}}$, MW/m	$\Delta\dot{H}$, MW/m	$P_{\text{MHD}} - P_b$, MW/m,	$\chi = P_{\text{MHD}}/H_{\text{inlet}}$, %
$M = 6$, $h = 27$ km	31	60	~0		
$M = 8$, no MHD	~27	85	~0		
$M = 8$, MHD $k = 0.5$	~27	81	3.7	3.5	4.5
$M = 8$, MHD $k = 0.9$	26.55	80	3	2.3	4.9

[a]All Mach 8 cases correspond to an altitude of 30 km.

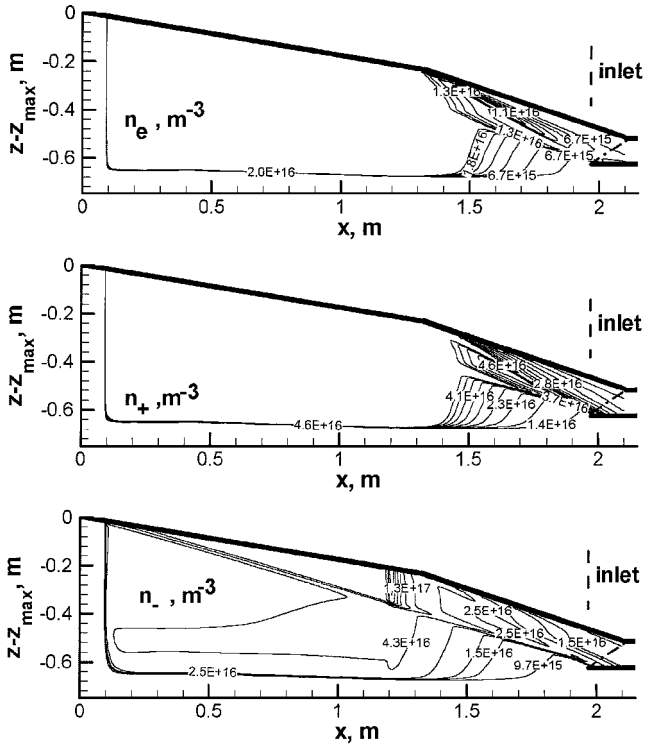

Fig. 9 Computed number densities charged species outside of the MHD region for the case shown in Fig. 7.

between the MHD-generated electrical power and the electron beam power $P_{\text{MHD}} - P_b$; and the ratio between the MHD-generated electrical power and the total enthalpy entering the inlet per unit time χ. All of these quantities are calculated per unit length in y direction. Mass flow into the inlet can be seen to be slightly lower with the stronger MHD effect, due to some deflection and displacement of the streamlines in the MHD region. This, plus the MHD power extraction from the flow, is responsible for the $\Delta\dot{H}$ being substantial and even slightly greater than $P_{\text{MHD}} - P_b$. The MHD-generated electrical power in both MHD cases constitutes about 4.5–5% of the enthalpy flux into the inlet.

Table 3 shows the variation of the major computed quantities with the change in grid size from 125 × 75 to 250 × 150. The variation is small, within 1–2% for all computed quantities. Thus, the accuracy of computed quantities is determined mostly by the 10–20% error of the simplified representation of electron beam power deposition profiles (see subsection II.C). Of course, the assumptions of an ideal Faraday generator and inviscid flow were also made in calculations, and errors introduced by these assumptions could be quantified in future, after relaxing these assumptions and performing more realistic modeling.

The issue of scaling of the computed results to larger geometric dimensions is important. If viscous, chemical, and vibrational-nonequilibrium effects are neglected, then, with an increase in all linear dimensions by, for example, a factor of 10, the same shock control effect would be accomplished if the MHD interaction parameter stays the same as in the computed two cases, $S = 0.11$ at $k = 0.5$ and $S = 0.17$ at $k = 0.9$. Thus, when electron beam current density and the magnetic field are kept constant, the length of

Table 3 Variation of the computed parameters with the grid size in the Mach 8 case with MHD and $k = 0.5$

Grid size	p_{tot}, 10^5 Pa	P_b, MW/m	P_{MHD}, MW/m	$P_{j\times B}$, MW/m	P_J, MW/m	P_v, MW/m	P_{VT}, MW/m
250 × 150	2.017	0.121	3.65	7.3	2.21	1.44	0.0784
125 × 75	2.05	0.121	3.6	7.12	2.14	1.38	0.07

MHD region should also stay constant, becoming a smaller fraction of the total forebody length. However, boundary-layer growth upstream and downstream of the MHD region, shock/boundary-layer interactions, and vibrational relaxation can be expected to be more pronounced in scaled-up geometry.

Conclusions

The paper presents a preliminary assessment of the possibility of controlling scramjet inlets in offdesign conditions by operating a near-surface MHD system upstream of the inlet. We have suggested the creation of electrical conductivity that is needed for MHD operation in cold air by electron beams injected from the vehicle. We have developed a simple model of beam-generated ionization profiles and coupled this model with plasma kinetics, MHD equations, and two-dimensional inviscid flow equations. Calculations demonstrated that an MHD system with reasonable parameters could bring shocks back to the cowl lip when flying at Mach numbers higher than those for which the inlet was optimized. The MHD effect is not reduced to heating only because the work by $\boldsymbol{j} \times \boldsymbol{B}$ forces is a substantial part of the overall effect. In computed cases, power requirements for ionizing electron beams are lower than the electrical power extracted with MHD, so that a net power would be generated onboard. In future work, the modeling could be coupled with a turbulent boundary-layer model, shock reflections and shock–shock interactions could be computed, and computations could be performed for full-scale systems. Among technical issues critical for cold-air hypersonic MHD operation are the following: electron beam injection and window/foil survivability and the threshold Hall field for the onset of arcing between electrode segments.

Acknowledgments

This work was supported by the Air Force Office of Scientific Research. The authors are also grateful to L. Martinelli for valuable discussions.

References

[1]Fraishtadt, V. L., Kuranov, A. L., and Sheikin, E. G., "Use of MHD Systems in Hypersonic Aircraft," *Technical Physics*, Vol. 43, No. 11, 1998, p. 1309.

[2]Gurijanov, E. P., and Harsha, P. T., "AJAX: New Directions in Hypersonic Technology," AIAA Paper 96-4609, 1996.

[3]Bityurin, V. A., Lineberry, J. T., Potebnia, V. G., Alferov, V. I., Kuranov, A. L., and Sheikin, E. G., "Assessment of Hypersonic MHD Concepts," AIAA Paper 97-2323, 1997.

[4]Bityurin, V. A., Klimov, A. I., Leonov, S. B., Bocharov, A. N., and Lineberry, J. T., "Assessment of a Concept of Advanced Flow/Flight Control for Hypersonic Flights in Atmosphere," AIAA Paper 99-4820, 1999.

[5]Brichkin, D. I., Kuranov, A. L., and Sheikin, E. G., "MHD Technology for Scramjet Control," AIAA Paper 98-1642, 1998.

[6]Kuranov, A. L., and Sheikin, E. G., "The Potential of MHD Control for Improving Scramjet Performance," AIAA Paper 99-3535, 1999.

[7]Brichkin, D. I., Kuranov, A. L., and Sheikin, E. G., "The Potentialities of MHD Control for Improving Scramjet Performance," AIAA Paper 99-4969, 1999.

[8]Macheret, S. O., Shneider, M. N., and Miles, R. B., "Electron Beam Generated Plasmas in Hypersonic MHD Channels," AIAA Paper 99-3635, June 1999.

[9]Macheret, S. O., Shneider, M. N., Miles, R. B., and Lipinski, R. J., "Electron Beam Generated Plasmas in Hypersonic Magnetohydrodynamic Channels," *AIAA Journal*, Vol. 39, No. 6, 2001, pp. 1127–1138.

[10]Macheret, S. O., Shneider, M. N., and Miles, R. B., "MHD Power Extraction From Cold Hypersonic Air Flows with External Ionizers," AIAA Paper 99-4800, Nov. 1999.

[11]Macheret, S. O., Shneider, M. N., and Miles, R. B., "Potential Performance of Supersonic MHD Power Generators," AIAA Paper 2001-0795, Jan. 2001.

[12]Chase, R. L., Mehta, U. B., Bogdanoff, D. W., Park, C., Lawrence, S., Aftosmis, M., Macheret, S. O., and Shneider, M. N., "Comments on an MHD Energy Bypass Engine Powered Spaceliner," AIAA Paper 99-4965, Nov. 1999.

[13]Park, C., Mehta, U. B., and Bogdanoff, D. W., "Real Gas Calculation of MHD-Bypass Scramjet Performance," AIAA Paper 2000-3702, 2000.

[14]Golovachev, Y. P., and Sushikh, S. Y., "Supersonic Air-Scoop Flows of a Weakly Ionized Gas in External Electromagnetic Field," *Technical Physics*, Vol. 45, No. 2, 2000, p. 168.

[15]Golovachev, Y. P., Sushikh, S. Y., and Van Wie, D., "Numerical Simulation of MGD Flows in Supersonic Media," AIAA Paper 2000-2666, 2000.

[16]Vatazhin, A., Kopchenov, V., and Gouskov, O., "Some Estimations of Possibility to Use the MHD Control for Hypersonic Flow Deceleration," AIAA Paper 99-4972, 1999.

[17]Kopchenov, V., Vatazhin, A., and Gouskov, O., "Estimation of Possibility of Use of MHD Control in Scramjet," AIAA Paper 99-4971, 1999.

[18]Vatazhin, A., Kopchenov, V., and Gouskov, O., "Numerical Investigation of Hypersonic Inlets Control by Magnetic Field," *2nd Workshop on Magneto- and Plasma Aerodynamics in Aerospace Applications*, Inst. of High Temperatures, Russian Academy of Sciences, Moscow, 2000, pp. 56–63.

[19]Shneider, M. N., Macheret, S. O., and Miles, R. B., "Electrode Sheaths and Boundary Layers in Hypersonic MHD Channels," AIAA Paper 99-3532, June 1999.

[20]Macheret, S. O., Miles, R. B., and Nelson, G. L., "Feasibility Study of a Hybrid MHD/Radiatively Driven Facility for Hypersonic Ground Testing," AIAA Paper 97-2429, June 1997.

[21]Macheret, S. O., Shneider, M. N., Miles, R. B., Lipinski, R. J., and Nelson, G. L., "MHD Acceleration of Supersonic Airflows Using Electron Beam Enhanced Conductivity," AIAA Paper 98-2922, June 1998.

[22]Macheret, S. O., Shneider, M. N., and Miles, R. B., "Modeling of Air Plasma Generation by Electron Beams and High-Voltage Pulses," AIAA Paper 2000-2569, June 2000.

[23]Aleksandrov, N. L., Vysikailo, F. I., Islamov, R. S., Kochetov, I. V., Napartovich, A. P., and Pevgov, V. G., "Electron Distribution Function in 4:1 N_2–O_2 Mixture," *High Temperature*, Vol. 19, No. 1, 1981, p. 17.

[24]Rosa, R. J., *Magnetohydrodynamic Energy Conversion*, McGraw–Hill, New York, 1968, Chaps. 3, 4.

[25]Anderson, D. A., Tannehill, J. C., and Pletcher, R., *Computational Fluid Mechanics and Heat Transfer*, Hemisphere, New York, 1984, Chap. 5.

[26]Kossyi, I. A., Kostinsky, A. Y., Matveyev, A. A., and Silakov, V. P., "Kinetic Scheme of the Non-Equilibrium Discharge in Nitrogen–Oxygen Mixtures," *Plasma Sources Science and Technology*, Vol. 1, No. 3, 1992, p. 207.

[27]Bazelyan, E. M., and Raizer, Y. P., *Spark Discharge*, CRC Press, Boca Raton, FL, 1997, Chap. 2.

[28]Raizer, Y. P., and Shneider, M. N., "Simplified Kinetic Equation for Electrons in Nonuniform Fields of Arbitrary Strength in Connection with the Cathode Sheath of a Glow Discharge," *Soviet Journal of Plasma Physics*, Vol. 15, No. 3, 1989, pp. 184–189.

[29]Berger, M. J., and Seltzer, S. M., "Tables of Energy Losses and Ranges of Electrons and Positrons," NASA SP-3012, 1964.

[30]Bychkov, Y. I., Korolev, Y. D., and Mesyats, G. A., *Injection Gaseous Electronics (Inzhektsionnaia Gazovaia Elektronika)*, Nauka, Moscow, 1982, Chap. 2 (in Russian).

P. Givi
Associate Editor